OXFORD

SOT | Society of Toxicology
www.toxsci.oxfordjournals.org

TOXICOLOGICAL SCIENCES, 169(2), 2019, 524–533

doi: 10.1093/toxsci/kfz064
Advance Access Publication Date: March 7, 2019
Research Article

Maternal Engineered Nanomaterial Inhalation During Gestation Disrupts Vascular Kisspeptin Reactivity

Elizabeth C. Bowdridge,*,† Alaeddin B. Abukabda,*,† Kevin J. Engles,* Carroll R. McBride,*,† Thomas P. Batchelor,*,† William T. Goldsmith,*,† Krista L. Garner,*,† Sherri Friend,‡ and Timothy R. Nurkiewicz*,†,‡,1

*Department of Physiology and Pharmacology; †Center for Inhalation Toxicology, Toxicology Working Group, West Virginia University School of Medicine, 26506; and ‡Health Effects Laboratory Division, National Institute for Occupational Safety and Health, Morgantown 26505, West Virginia

[1]To whom correspondence should be addressed at Department of Physiology and Pharmacology, Robert C. Byrd Health Sciences Center, West Virginia University, 64 Medical Center Drive, Morgantown 26505, WV 26505-9229. Fax: (304) 293-5513. E-mail: tnurkiewicz@hsc.wvu.edu.

Disclaimer: The findings and conclusions in this report are those of the author(s) and do not necessarily represent the official position of the National Institute for Occupational Safety and Health, Centers for Disease Control and Prevention.

ABSTRACT

Maternal engineered nanomaterial (ENM) inhalation is associated with uterine vascular impairments and endocrine disruption that may lead to altered gestational outcomes. We have shown that nano-titanium dioxide (nano-TiO_2) inhalation impairs endothelium-dependent uterine arteriolar dilation in pregnant rats. However, the mechanism underlying this dysfunction is unknown. Due to its role as a potent vasoconstrictor and essential reproductive hormone, we examined how kisspeptin is involved in nano-TiO_2-induced vascular dysfunction and placental efficiency. Pregnant Sprague Dawley rats were exposed (gestational day [GD] 10) to nano-TiO_2 aerosols (cumulative dose = 525 ± 16 μg; $n = 8$) or sham exposed ($n = 6$) and sacrificed on GD 20. Plasma was collected to evaluate estrogen (E_2), progesterone (P4), prolactin (PRL), corticosterone (CORT), and kisspeptin. Pup and placental weights were measured to calculate placental efficiency (grams fetus/gram placental). Additionally, pressure myography was used to determine uterine artery vascular reactivity. Contractile responses were assessed via cumulative additions of kisspeptin (1×10^{-9} to 1×10^{-4} M). Estrogen was decreased at GD 20 in exposed (11.08 ± 3 pg/ml) versus sham-control rats (66.97 ± 3 pg/ml), whereas there were no differences in P4, PRL, CORT, or kisspeptin. Placental weights were increased in exposed (0.99 ± 0.03 g) versus sham-control rats (0.70 ± 0.04 g), whereas pup weights (4.01 ± 0.47 g vs 4.15 ± 0.15 g) and placental efficiency (4.5 ± 0.2 vs 6.4 ± 0.5) were decreased in exposed rats. Maternal ENM inhalation exposure augmented uterine artery vasoconstrictor responses to kisspeptin (91.2%±2.0 vs 98.6%±0.10). These studies represent initial evidence that pulmonary maternal ENM exposure perturbs the normal gestational endocrine vascular axis via a kisspeptin-dependent mechanism, and decreased placental, which may adversely affect health outcomes.

Key words: engineered nanomaterials; titanium dioxide; microcirculation; kisspeptin; placenta.

The advancement of nanotechnology holds tremendous potential to improve human health (Hendren *et al.*, 2011). However, our understanding of the health effects of unintended exposures to these materials is poor. Perhaps of greater concern is the maternal fetal outcomes of gestation inhalation exposure. Maternal engineered nanomaterial (ENM) inhalation during gestation is associated with uterine vascular impairments (Stapleton, 2013) and endocrine disruptions (Larson *et al.*, 2014) that may lead to altered gestational outcomes. One of the most prolifically used nanomaterials is nano-TiO_2. Nano-TiO_2 is also industrially widespread in building materials, filters and is used as a carrier to deliver nanomedicines. We have

previously established that nano-TiO_2 inhalation exposure impairs uterine microcirculation of both virgin and pregnant rats (Stapleton *et al.*, 2018). Inhalation is the primary exposure route through which ENM exposures occur, however, the role of maternal ENM inhalation exposure as endocrine disruptors during gestation has not been well explored.

Negative endocrine and gestational outcomes have been shown with intragastric (Gao *et al.*, 2012; Ramsden *et al.*, 2013) and intravenous injection (Yamashita *et al.*, 2011) of nano-TiO_2. However, it remains to be determined how maternal ENM inhalation during gestation adversely affects reproductive and endocrine outcomes. In one case, maternal inhalation exposure to silver nanoparticles during gestation in mice resulted in decreased plasma E_2 and increased fetal resorptions (Campagnolo *et al.*, 2017). Additionally, we have reported that maternal nano-TiO_2 inhalation during gestation impairs endothelium-dependent uterine arteriolar dilation (Stapleton *et al.*, 2018). Considered together, this strongly implies that normal uterine vascular function and/or adaptations and the endocrine milieu are disrupted as a result of maternal ENM inhalation during gestation. However, the link between the mechanisms underlying this vascular and endocrine dysfunction has yet to be fully determined.

Gestation is a period of rapid maternal and fetal microvascular growth (Mandala and Osol, 2012; Osol and Mandala, 2009; Reynolds and Redmer, 1992), and these vessels are particularly sensitive to a host of toxicants. Thus, there is a tremendous need to define the potentially harmful effects of maternal ENM inhalation exposure. According to Barker's hypothesis on the developmental origins of health and disease (DOHaD), compromised vascular function and/or adaptation to the increased demand for blood flow during development may create a hostile gestational environment, or a "utero-placental insufficiency" that forms the basis for adult disease (Barker, 1990; Barker and Martyn, 1992). This is important because ENMs are present in diverse application ranging from consumer products to novel therapeutics. Although it is difficult to accurately quantify data about industrial ENM burdens, annual estimated projections exist and in 2011, titanium dioxide was one of the five most prolific ENM of which nano-TiO_2 dominated with ~38 000 tons (Hendren *et al.*, 2011). Inhalation is the most common route of unintended nanomaterial exposures. However, consequences of ENM inhalation exposure on maternal and fetal cardiovascular health during gestation are largely unknown. Therefore, identifying these conditions and consequences of maternal ENM exposures during gestation would constitute a major step toward: (1) the protection of maternal-fetal health; and (2) identifying safe ENM exposure conditions and characteristics that significantly protect and/or improve human health.

Kisspeptin is a member of the RF-amide peptide family, which have a distinct terminal -Arg- Phe-NH_2 (Qaiser *et al.*, 2012), are evolutionarily conserved from invertebrates to mammals and have been shown to have important physiological roles in reproduction (d'Anglemont de Tassigny and Colledge, 2010) and energy balance (Castellano *et al.*, 2010). Kiss has been shown to have key roles in reproduction including trophoblast invasion (Kotani *et al.*, 2001), and being a neuropeptide critical for puberty (Bilban *et al.*, 2004) and fertility (de Roux *et al.*, 2003). In addition, altered Kiss signaling is associated with several vascular-based complications such as hypertension, pre-eclampsia, and intrauterine growth restriction (IUGR) during gestation (Cetković *et al.*, 2012). According to the National Institute of Environmental Health Sciences (NIEHS) in 2013, the incidence of adverse pregnancy outcomes due to exposure to endocrine disrupting chemicals is on the rise. Thus, the effects of exposure to harmful materials during sensitive windows of fetal development still require careful scrutiny.

Despite its association with various gestational complications, the role of Kiss signaling and its downstream effects on vascular health during gestation have never been considered concerning any toxicant exposure. The vasoactive effects of Kiss have only been observed in a macrovascular preparation resulting in vascular smooth muscle contraction in human aorta and coronary artery (Mead *et al.*, 2007). This approach does not directly evaluate vascular resistance within a given tissue. As such, the influences of Kiss on uterine microvascular reactivity during gestation are unknown. One possibility is alterations in the steroid hormone E_2, which is elevated and critical for a healthy pregnancy, affects Kiss, which is a potent vasoconstrictor.

Therefore, we examined how circulating E_2 and Kiss are involved in nano-TiO_2-induced vascular dysfunction. We hypothesized that maternal ENM inhalation exposure during gestation would decrease E_2 thereby augmenting the vasoconstrictive effects of Kiss on the uterine vasculature. Additionally, we hypothesized that maternal ENM exposure-induced endocrine disruption of estrogen and/or kisspeptin influences that lead to increased vasoconstriction and therefore reduced fetal growth and placental efficiency.

MATERIALS AND METHODS

Animal model. Female Sprague Dawley (SD rats) were purchased from Hilltop Laboratories (Scottdale, Pennsylvania), and housed in an Assessment and Accreditation of Laboratory Animal Care (AAALAC) approved facility at West Virginia University (WVU) under a regulated temperature and 12:12 h light-dark cycle. Rats were randomly assigned to either the sham-control or nano-TiO_2-exposure groups and acclimated for 48–72 h before mating. Rats had *ad libitum* access to food and water throughout the acclimation period. To increase the likelihood of viable progeny, pregnant rats were exposed on or after implantation (GD 10) as prior indications of inhalation exposure results in near to total loss of pregnancy. Weights of the pregnant dams were recorded weekly. Twenty-four hours after the last exposure, dams were sacrificed on GD 20. All procedures were approved by the Institutional Animal Care and Use Committee of West Virginia University.

Engineered nanomaterial. Nano-TiO_2 powder was obtained from Evonik (Aeroxide TiO_2, Parsippany, New Jersey). It is a mixture composed of anatase (80%) and rutile (20%) TiO_2. Particle characteristics have been determined including the primary particle size (21 nm), the specific surface area (48.08 m^2/g) (Stapleton *et al.*, 2018), and the Zeta potential (−56.6 mV).

Inhalation exposure. Nano-TiO_2 aerosols were generated using a high-pressure acoustical generator (HPAG, IEStechno, Morgantown, West Virginia). The output of the generator was fed into a Venturi pump (JS-60M, Vaccon, Medway, Massachusetts), which further de-agglomerated the particles. The nano-TiO_2 aerosol/air mix then entered the whole-body exposure chamber. A personal DataRAM (pDR-1500; Thermo Environmental Instruments Inc., Franklin, Massachusetts) was utilized to sample the exposure chamber air to determine the aerosol mass concentration in real time. Feedback loops within the software automatically adjusted the acoustic energy to

maintain a stable mass concentration during the exposure. Gravimetric measurements were conducted on Teflon filters concurrently with the DataRAM measurements to obtain a calibration factor. The gravimetric measurements were also conducted during each exposure to calculate the mass concentration measurements reported in the study. Bedding material soaked with water was used in the exposure chamber to maintain comfortable humidity (30%–70%) during exposures. Sham-control animals were exposed to HEPA-filtered air only with similar temperature and humidity chamber conditions. Aerosol size distributions were measured from the exposure chamber whereas the mass concentration was being maintained at 12 mg/m^3 with: (1) a high-resolution electrical low-pressure impactor (ELPI+; Dekati, Tampere, Finland), (2) a scanning particle mobility sizer (SMPS 3938; TSI Inc., St. Paul, Minnesota), and (3) an aerodynamic particle sizer (APS 3321; TSI Inc., St. Paul, Minnesota).

Inhalation exposures lasted for 6 days after GD 10 to decrease animal stress. The pregnant rats were exposed to an average target concentration of 12 mg/m^3. This concentration was chosen to match our previous late gestation inhalation exposure studies (Stapleton *et al.*, 2013, 2018; Stapleton and Nurkiewicz, 2014). To estimate lung dose with ultrafine TiO_2 aerosols (Nurkiewicz *et al.*, 2008), we used the equation: $D = F{\cdot}V{\cdot}C{\cdot}T$, where F is the deposition fraction (10%), V is the minute ventilation (208.3 cc), C equals the mass concentration (mg/m^3), and T equals the exposure duration (minutes) (Yi *et al.*, 2013). This exposure paradigm (12 mg/m^3, 6 h/exposure, 6 days) produced an estimated target lung dose of 525 ± 16 μg with the last exposure conducted 24 h prior to sacrifice and experimentation. These calculations represent total lung deposition and do not account for clearance (MPPD Software v 2.11, Arlington, Virginia).

Enzyme-linked immunosorbent assay (ELISA). Rats were anesthetized with isoflurane gas (5% induction, 2%–3.5% maintenance). The animals were placed on a heating pad to maintain a 37°C rectal temperature. The trachea was intubated to ensure an open airway and the right carotid artery was cannulated to allow for blood sampling of ~3 ml. Plasma was collected on GD 20 and ELISAs were performed for E_2, P4, LH, FSH, PRL CORT, and Kiss. All kits were performed according to the recommendation of the manufacturer (CalBiotech, Spring Valley, California).

Pup weight, placenta weights, and placental efficiency. After blood collection, pups and placenta were dissected out of the uterus and weighed individually. Pup and placental weights were measured to calculate placental efficiency (grams fetus/gram placental).

Isolated microvessel protocol: pressure myography microvessel preparation. Once the pups and placenta were removed, uteri were placed in a dissecting dish with physiological salt solution (PSS) maintained at 4°C. A segment of the uterine artery was isolated, removed, transferred to a vessel chamber (Living Systems Instrumentation, Burlington, Vermont) containing fresh oxygenated PSS, cannulated with glass pipettes, and secured using nylon suture (11-0 ophthalmic, Alcon, United Kingdom). Arterioles were extended to their *in situ* length, pressurized to 60 mm Hg with PSS, superfused with warmed (37°C) oxygenated PSS at a rate of 10 ml/min, and allowed to develop spontaneous tone. Internal and external arteriolar diameters were measured using video calipers (Colorado Video, Boulder, Colorado).

Uterine reactivity. Uterine arteries were allowed to develop spontaneous tone, defined as the degree of constriction experienced by a blood vessel relative to its maximally dilated state. Vascular tone ranges from 0% (maximally dilated) to 100% (maximal constriction). Vessels with a spontaneous tone ≥20% less than initial tone were included in this study. After equilibration, parameters of arterial vasoreactivity were analyzed. Vessels that did not develop sufficient spontaneous tone were not included in the data analysis.

Assessment of vasoreactivity. Arteries were exposed to increasing concentrations of acetylcholine (ACh: 10^{-9}–10^{-4} M), sodium nitroprusside (SNP: 10^{-9}–10^{-4} M), kisspeptin-10 (Kiss: 10^{-9}–10^{-4} M), and phenylephrine (PE: 10^{-9}–10^{-4} M) which were each added separately to the chamber. The steady-state diameter of the vessel was recorded for at least 2 min after each dose. After each dose curve was completed, the vessel chamber was washed to remove excess chemicals by carefully removing the superfusate and replacing it with fresh warmed oxygenated PSS. After all experimental treatments were complete, the PSS was replaced with Ca^{2+}-free PSS until maximum passive diameter was established. All arteries with <20% spontaneous tone were not analyzed.

Pressure myography calculations. Data are expressed as means ± standard error. Spontaneous tone was calculated by the following equation:

$$\text{Spontaneous tone } (\%) = \left\{\frac{(D_m - D_i)}{D_i}\right\} \times 100$$

where D_m is the maximal diameter and D_i is the initial steady-state diameter recorded prior to the experiment. Active responses to pressure were normalized to the maximal diameter using the following formula:

$$\text{Normalized diameter} = D_{ss}/D_m$$

where D_{SS} is the steady-state diameter recorded during each pressure change. The experimental responses to ACh, PE, and SNP are expressed using the following equation:

$$\text{Diameter(percent maximal diameter)} = \left\{\frac{(D_{ss} - D_{con})}{(D_m - D_{con})}\right\} \times 100$$

where D_{con} is the control diameter recorded prior to the dose curve, D_{SS} is the steady-state diameter at each dose of the curve. The experimental response to PE is expressed using the following equation:

$$\text{Diameter(percent maximal diameter)} = \left\{\frac{(D_{con} - D_{ss})}{(D_{con})}\right\} \times 100$$

Wall thickness (W_T) was calculated from the measurement of both inner (ID) and outer (OD) steady state arteriolar diameters at the end of the Ca^{2+}-free wash using the following equation:

$$WT = (OD - ID)/2$$

Dual-label immunofluorescent detection of Kiss/Kiss1R and Von-Willebrand factor. Uteri were removed immediately after sacrifice and two placentas per rat were dissected away from the pup and uterine wall. Placental tissue was immediately placed into 4% paraformaldehyde fixative for 3 h at 4°C and transferred to

phosphate-buffered saline (PBS) overnight. Twelve hours later, the tissue was flash frozen and stored at −80°C until sectioned. Placentas were sectioned at 50 μm through the center of the placenta. Three sections per rat were analyzed for mean fluorescent intensity. On day 1 of the protocol, sections were washed 4 × 5 min in 0.1 M PBS to remove excess cryoprotectant and stored overnight at 4°C. The next day, sections were washed 4 × 5 min in PBS, placed in 1% H_2O_2 for 10 min and subsequently washed 4 × 5 min in PBS. Tissue was then incubated for at least 1 h in a blocking solution containing PBS, 0.4% Triton X-100 (PBSTX) (Sigma-Aldrich, St. Louis, Missouri) and 20% normal goat serum (NGS) (Jackson ImmunoResearch Laboratories, Inc., West Grove, Pennsylvania) in PBS. Tissue sections were placed in a solution containing rabbit anti-kisspeptin (no. AC566; a gift from A. Caraty, Universite' Tours, Nouzilly, France, dilution 1:40 000) or rabbit anti-kisspeptin receptor (AbCam, 1:500) in PBSTX and 20% NGS for 16 h. After incubation with the primary antibody, sections were incubated in a solution containing biotinylated goat anti-rabbit IgG and a solution containing avidin-biotin horseradish-peroxidase conjugate (Vectastain Elite ABC; dilution 1:600; Vector Laboratories) for 1 h. Sections were then washed and incubated for 10 min in biotinylated tyramine (TSA) (dilution 1:250; Perkin Elmer, Waltham, Massachusetts) in PBS containing 3% H_2O_2 per 1 ml of solution. After washing, sections were incubated in a solution containing DyLight green 488-streptavidin (1:200, Fisher Scientific) for 1 h followed by washes and incubation in PBSTX and 4% NGS for at least 1 h. Sections were incubated in mouse anti-smooth muscle actin (catalog number ab 7817; dilution 1:1000; AbCam, Cambridge, Massachusetts) or anti-Von Willebrand factor (catalog number ab6994; dilution 1:200) in PBSTX and 4% NGS for 16 h. The next day, sections were incubated in Alexa555 goat anti-rabbit (dilution 1:200; Life Technologies, Carlsbad, California) for 1 h, washed, mounted on Superfrost slides (Fisher Scientific), coverslipped using ProLong Diamond Antifade Mountant with DAPI (Thermo Fisher, Waltham, Massachusetts) and stored in the dark at 4°C until analysis.

Statistics. Point-to-point differences in the dose-response curves were evaluated using 2-way repeated measures analysis of variance (ANOVA) with a Tukey's post hoc analysis when significance was found. The animal characteristics, vessel characteristics, and dose-response curve slopes were analyzed using a 1-way ANOVA with a Tukey post hoc analysis when significance was found. All statistical analysis was completed with JMP Pro 12 (SAS Institute, Cary, North Carolina). Significance was set at $p < .05$, *N* is the number of animals per group, *n* is the number of vessels per group.

RESULTS

Scanning Electron Microscopy and Mass Spectrometry of Nano-TiO_2

The aerosol concentration of nano-TiO_2 was determined to be 10.35 ± 0.13 mg/m^3 (Figure 1A).The ELPI high-resolution data indicated a geometric count median diameter of 188 nm with a geometric standard deviation of 2.02 (Figure 1B). The SMPS and APS data were combined to determine the geometric count median diameter using the log normal distribution obtained with the log probability plot method and was determined to be 190 nm with a geometric standard deviation of 1.97 (Figure 1C). Figure 1D shows a representative transmission electron microscope (TEM) (JEOL 1400, JEOL Tokyo, Japan) image of a nano-TiO_2.

Uterine Artery Characteristics

Sham-control and nano-TiO_2-exposed vessels had a similar inner (sham control = 350 ± 58 μm vs exposed = 203 ± 43 μm) and outer diameter (sham control = 511 ± 41 μm vs exposed = 454 ± 72 μm), however there was a trend for the tone to be increased in exposed uterine arteries (sham control = 26 ± 6 μm vs exposed = 46 ± 5 μm; $p = .6$; Table 1).

Pup Weight, Placenta Weights and Placental Efficiency

We have previously reported that the liter size, age, weight, and blood pressure of the dams was not different between groups (Abukabda *et al*., 2019). Pups born to dams exposed to nano-TiO_2 aerosols were significantly smaller (4.01 ± 0.47 g; $n = 73$ pups) when compared with sham-control (4.15 ± 0.15 g; $n = 46$ pups; $p < .05$) pups (Table 2). Nano-TiO_2 exposure also leads to an increase in placental weight (0.99 ± 0.03 g vs control 0.70 ± 0.04 g; $p < .05$). Therefore, the placental efficiency, which is calculated as grams fetus/grams placenta, in exposed rats was significantly decreased (4.52 ± 0.20) versus that of control rats (6.35 ± 0.50; $p < .05$).

Vasoreactivity Assessments

Kisspeptin incubation did not stimulate vasoreactivity in uterine arteries from sham-control rats (overall Δ = 1.08% diameter decrease). Whereas, uterine arteries from maternal nano-TiO_2 inhalation exposure group had a significantly responded with a vasoconstriction (Figure 2A, overall Δ = 15.14% diameter decrease). Therefore, pulmonary nano-TiO_2 exposure in pregnant rats augments vasoconstriction in response to Kiss. In contrast, no point-to-point differences were seen in α-adrenergic (Figure 2B) and endothelium independent (Figure 2C) or -dependent (Figure 2D) dilation between sham-control and nano-TiO_2-exposed groups.

Assessment of Plasma Hormones at Gestational Day 20

Plasma E_2 was significantly decreased at GD 20 in exposed (11.08 ± 2.5 pg/ml) versus sham-control rats (66.97 ± 2.5 pg/ml; $p < .05$; Figure 3A). This indicates that maternal nano-TiO_2 exposure causes endocrine disruption during pregnancy, which could lead to poor gestational and fetal outcomes. However, there was no difference between the groups in CORT levels (Figure 3B), indicating that exposure is not altering sex steroid concentrations through any undue stress. Additionally, there were no differences in P4 (Figure 3C), Kiss (Figure 4A), FSH (Figure 4B), LH (Figure 4C), and PRL (Figure 4D).

Placental Histology

We first examined colocalization of Kiss1R in the endothelial layer of the microcirculation (Figure 5A). Immunohistochemical analysis of Kiss1R (red) and Von-Willebrand Factor (green), a marker for endothelial and platelet cells, in large vessels from a nonpregnant uterus revealed that Kiss1R is adjacent to the endothelium and there is no colocalization. We then verified the presence of Kiss1R in the uterine microcirculation (Figure 5B). Immunohistochemical analysis of Kiss1R (red) and α-smooth muscle actin (green), a marker for smooth muscle cells, in vessels in a nonpregnant uterus revealed areas of colocalization indicating that Kiss1R is expressed in the tunica media vascular layer surrounding uterine arterioles. Next, we confirmed that Kiss was present in rat placental vasculature at GD 20 (Figure 6). Together, this reflects that the membrane bound G-protein receptor, Kiss1R, is located in the smooth muscle layer of uterine vessels, and that the peptide, Kiss, is produced by the rat placenta during late gestation.

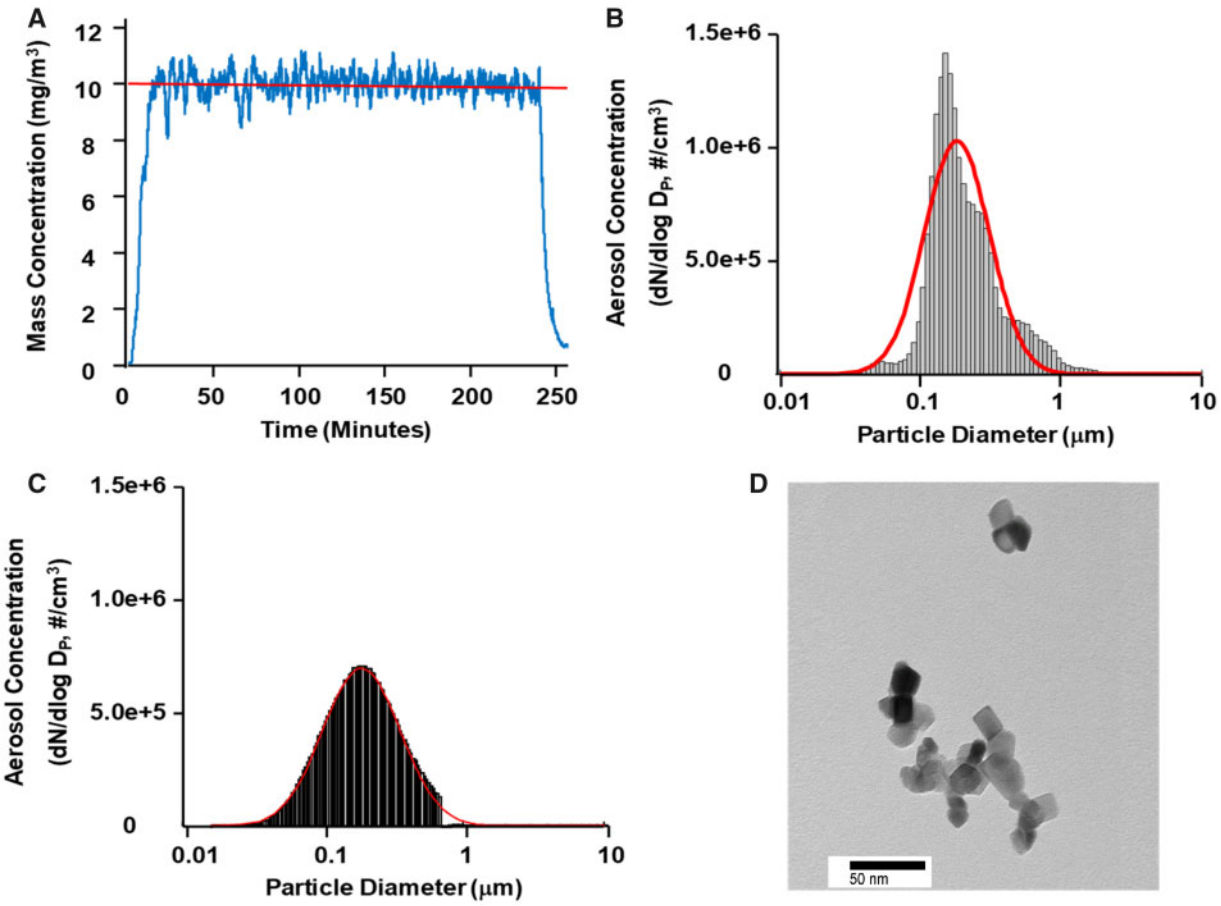

Figure 1. Characterization of nano-TiO_2. A, Real-time mass concentration measurements of the nano-TiO_2 aerosol during a typical inhalation exposure. The red line represents the target concentration, ~12 mg/m^3. B, Size distribution of the nano-TiO_2 aerosol (aerodynamic diameter) using a high-resolution electrical low-pressure impactor (ELPI+). The red line represents a log-normal fit of the histogram (count median diameter = 188 ± 0.36 nm). C, Size distribution of the nano-TiO_2 aerosol (mobility diameter) sampled from the exposure chamber using a scanning mobility particle sizer (SMPS—light gray) and an aerodynamic particle sizer (APS—dark gray, negligible values). The red line is representative of a log-normal fit of the histogram (count median diameter = 190 nm). D, Transmission electron microscope (TEM) image of a typical nano-TiO_2 agglomerate.

Table 1. Uterine Artery Characteristics

	n	Inner Diameter (μm)	Wall Thickness (μm)	Tone (%)	Passive Outer Diameter (μm)	Passive Wall Thickness (μm)
Sham control	8	350 ± 58	50 ± 4	26 ± 6	511 ± 41	54 ± 11
Nano-TiO_2 exposed	7	203 ± 43[a]	54 ± 17	46 ± 5[a]	454 ± 72	73 ± 15

Uterine artery characteristics in sham-control ($n = 8$) and inhalation-exposed ($n = 7$) groups. Values are shown as mean ± SEM. Statistics were analyzed with 1-way ANOVA ($p \leq .10$).
[a]Sham-control group versus nano-TiO_2-exposed groups.

Table 2. Pup and Placental Characteristics

	N	Pup Wet Weight (g)	Placental Wet Weight (g)	Placental Efficiency (grams fetus/grams placenta)	Pup Dry Weight (g)	Placenta Dry Weight (g)	Placental Efficiency (grams fetus/grams placenta)
Sham control	8	4.15 ± 0.15	0.70 ± 0.04	6.35 ± 0.50	0.56 ± 0.03	0.12 ± 0.007	4.83 ± 0.34
Nano-TiO_2 exposed	7	4.01 ± 0.47[a]	0.99 ± 0.03[a]	4.52 ± 0.20[a]	0.50 ± 0.02[a]	0.11 ± 0.002[a]	4.66 ± 0.22

Pup and placental characteristics in sham-control ($N = 8$) and nano-TiO_2 inhalation-exposed ($N = 7$) groups. Values are shown as mean ± SEM. Statistics were analyzed with 1-way ANOVA ($p \leq .05$).
[a]Sham-control group versus nano-TiO_2-exposed groups.

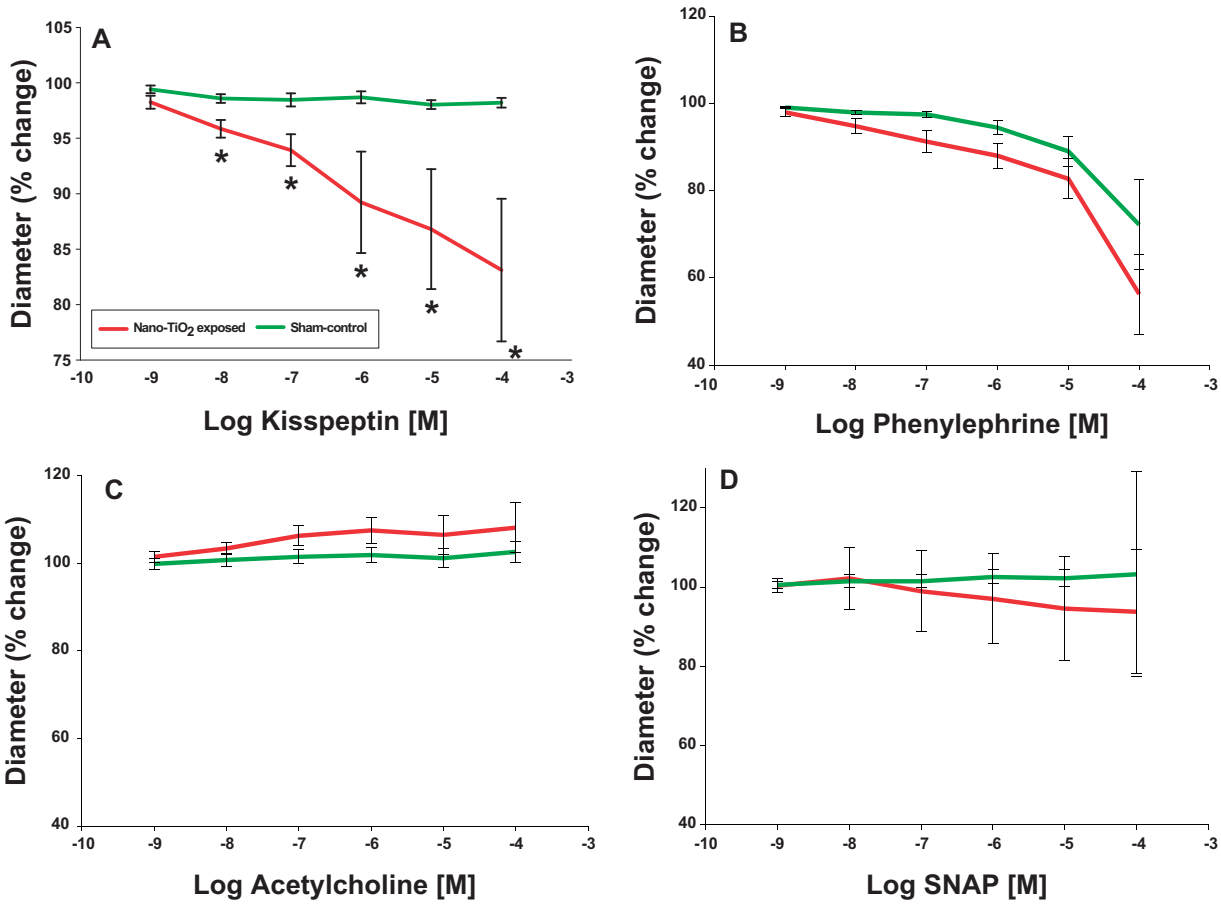

Figure 2. Kisspeptin induces constriction in uterine arteries exposed to nano-TiO_2. Kiss-dependent reactivity of uterine arteries from control and exposed animals was determined using pressure myography (N = 7–8). Statistics were analyzed with 1-way ANOVA ($p \leq .05$). *Sham-control group versus nano-TiO_2-exposed groups.

DISCUSSION

These studies represent the first evidence that maternal ENM exposure perturbs the normal gestational endocrine vascular axis, which is characterized by an augmented vascular Kiss reactivity. Kiss treatment of uterine arteries from dams exposed to nano-TiO_2 during gestation resulted in a significant increase in constriction when compared with sham controls (Figure 2). Binding of Kiss to its cognate G-protein-coupled receptor, Kiss1R, signals via $G_{\alpha q/11}$ to trigger activation of phospholipase beta, cause hydrolysis of phosphatidylinositol 4,5-bisphosphate to diacylglycerol and inositol triphosphate, and mobilize intracellular calcium, which leads to smooth muscle contraction (Millar and Babwah, 2015). The change in vasoconstriction (quantified as % Δ = control diameter-Kiss diameter) for sham-control and nano-TiO_2 aerosol-exposed uterine arteries from GD 20 in response to Kiss is shown in Figure 2. An increase in vasoconstriction was seen in exposed uterine arteries (overall Δ = 15.14% diameter decrease). In contrast, no change in vasoconstriction was seen in sham controls (overall Δ = 1.08% diameter decrease). Therefore, pulmonary nano-TiO_2 exposure in pregnant rats augments vasoconstriction in response to Kiss. Sham-control and exposed vessels had a similar inner (sham control = 350 ± 58 μm vs exposed = 203 ± 43 μm) and outer diameter (sham control = 511 ± 41 μm vs exposed = 454 ± 72 μm), however there was a trend for the tone to be increased in uterine arteries from exposed dams (sham control = 26 ± 6 μm vs exposed = 46 ± 5 μm; $p = .6$). Importantly, the response to Kiss was augmented by nano-TiO_2 exposure. This provides strong evidence that Kiss1R is present in the rat placental vasculature and that pulmonary nano-TiO_2 exposure augments the influence of Kiss on vasoconstriction.

After observing the impact of nano-TiO_2 on microvascular dysfunction, we then sought to determine if maternal exposure induces endocrine disruption during gestation. We saw that ENM exposure leads to endocrine disruption. Plasma E_2 levels are shown in Figure 3A. Of note is the significant reduction in plasma E_2 at GD 20 in exposed rats versus sham control. This indicates that maternal nano-TiO_2 inhalation exposure causes endocrine disruption during pregnancy, which could lead to poor gestational and fetal outcomes. Poor follicular and oocyte development outcomes, which are also influenced by E_2 levels, were seen in rat preantral follicles subjected to increasing doses of nano-TiO_2. *In vitro* exposure led to inhibition of follicular development and oocyte maturation, and decreased survival rate of follicles, formation of antral follicles, and release of cumulus-oocyte complexes (Hou *et al.*, 2009). However, there was no difference between the groups in corticosterone levels (Figure 3B), indicating that exposure did not alter sex steroid concentrations on GD 20 through any undue stress. We also saw no differences in P4 or PRL on GD 20, which are also key hormones during gestation. Lastly, there were no differences in circulating levels of Kiss between sham-exposed and nano-TiO_2-exposed dams. This was not unexpected considering the human seems to be the only mammal in which circulating Kiss levels rise continuously throughout gestation until parturition

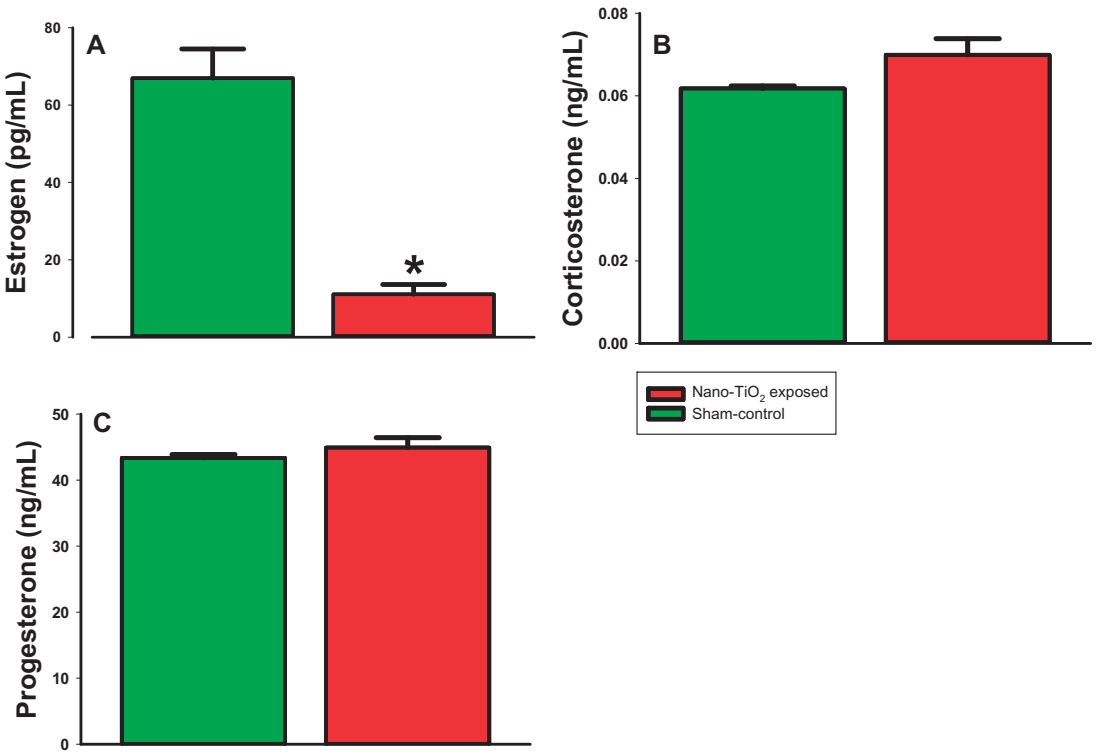

Figure 3. Plasma hormone analysis of steroid hormones at GD 20. ELISAs were performed on plasma from sham-control ($N = 6$) or nano-TiO_2 inhalation-exposed ($N = 6$) dams for (A) estrogen (E2), and (B) corticosterone (CORT), and (C) progesterone (P4). Statistics were analyzed with 1-way ANOVA ($p \leq .05$). *Sham-control group versus nano-TiO_2-exposed groups.

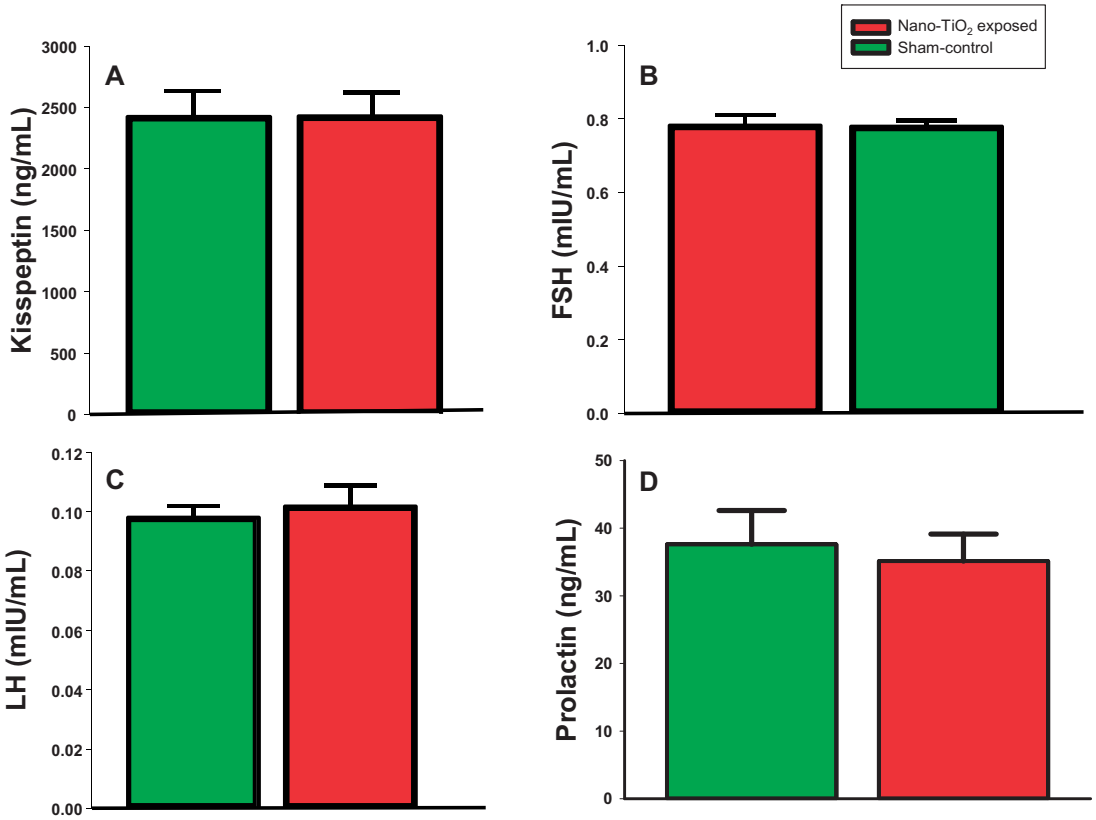

Figure 4. Plasma hormone analysis of peptide hormones at GD 20. ELISAs were performed on plasma from sham-control ($N = 6$) or nano-TiO_2 inhalation-exposed ($N = 6$) dams for (A) kisspeptin (E2), and (B) follicle-stimulating hormone (FSH), (C) luteinizing hormone (LH), and (D) prolactin (PRL). Statistics were analyzed with 1-way ANOVA.

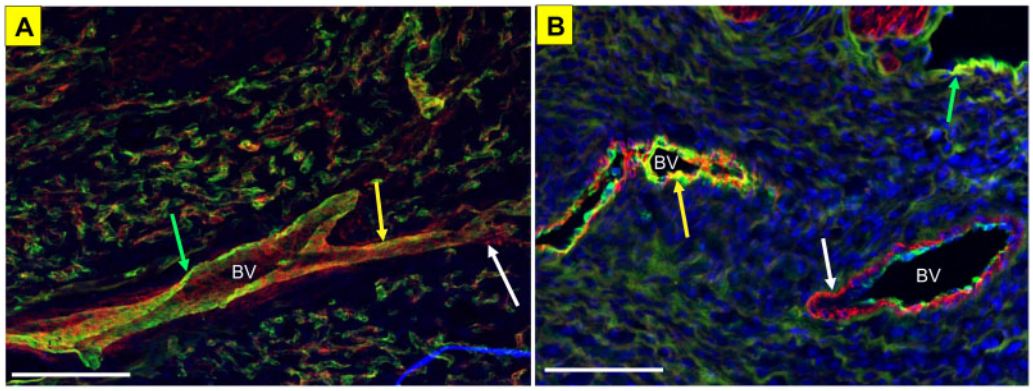

Figure 5. Kiss1R localization within the uterine and placental vasculature. Kiss1R (green) colocalization with SMA (red) in the mesometrial triangle (A), and within the placental vasculature (blood vessels indicated with BV) (B). Scale bar represents 100 μm for both panels; white arrow indicates positive staining for SMA, green arrow indicates positive staining for Kiss1R, and the yellow arrow indicates colocalization of Kiss1R and SMA.

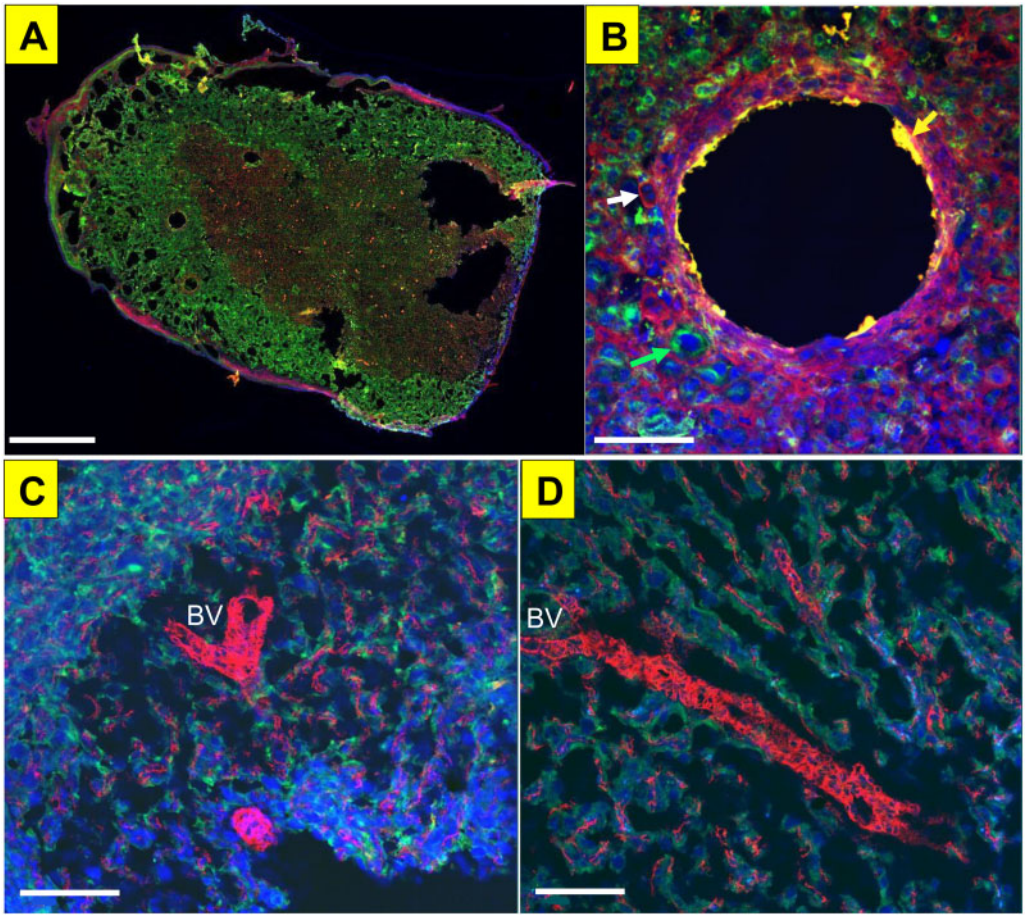

Figure 6. Kiss localization in the uterine and placental vasculature. Kiss (green) colocalization with α-smooth muscle actin (SMA, red) in placental microvessel (as seen in yellow), nuclear DAPI staining in blue in a whole placental slice (**A**), and magnification of an arteriole showing colocalization with SMA and Kiss (**B**; white arrow indicates positive staining for SMA, green arrow indicates positive staining for Kiss, and the yellow arrow indicates colocalization of Kiss and SMA). Kiss (green) trophoblast cells surrounding microvessels in the placenta indicated by SMA (red), however there is no colocalization between Kiss and SMA (**C**, **D**). Scale bar represents 1mm for panel A and 100 μm for panels B, C, D.

(Lehman *et al.*, 2018). However, it would be interesting to investigate local levels of Kiss in the uterine blood supply, which may be able to be determined by cannulating the draining vessels of the uterus.

Increased sensitivity of uterine vessels to the potent vasoconstrictor, Kiss, could lead to under perfusion or increased resistance of the uteroplacental unit *in vivo* in exposed dams. In our recent study, it was found that there was in fact increased resistance across the placentas on dams gestationally exposed to ENM (Abukabda *et al.*, 2019). Increases in placental resistance has been shown to lead to gestational complication such as

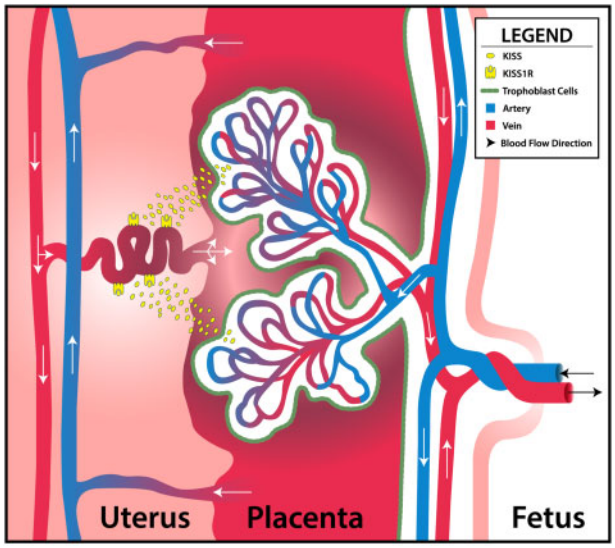

Figure 7. Proposed mechanism of action of kisspeptin within the uteroplacental unit in the rat during gestation. Kiss, which is synthesized by the trophoblast cells of the placenta, bind to Kiss1R in the arteries within the uterine wall. Exposure to ENM during gestation alters uterine vascular reactivity to Kiss, and potentially decreases blood flow to the placental units to decrease pup weight and increase placental weight.

IUGR and preeclampsia (Kotani *et al.*, 2001). Similar to this, we saw decreased pup weight and increased placental weight in dams exposed to nano-TiO_2 when compared with sham controls (Table 2). Changes in these two parameters also led to decreased placental efficiency in this exposed group. Placental efficiency is defined as grams of fetus produced per gram of placenta (Wilson and Ford, 2001). Insufficient placentas tend to occur when oxygen availability is limited by either poor placental vascularization (Fowden *et al.*, 2006) and/or reduced maternal blood flow. In this study, maternal ENM inhalation exposure may have limited oxygen availability through increased vasoconstriction and resistance across the placenta leading to smaller pups despite larger placental units.

We also revealed the presence of Kiss and its receptor, Kiss1R, in the rat placental vasculature at GD 20. Figure 5 shows the colocalization of Kiss1R with smooth muscle actin in the uterine vessels located in the mesometrial triangle, as well as in the smooth muscle cells in the microvessels of the placenta. In addition to Kiss1R being present in the uterus, Kiss production is colocalized to the smooth muscle layer surrounding placental vessels as well. Kiss has also been shown to be produced by the trophoblast cells in the placenta, which can also be seen in Figure 6. Together, this indicates that the membrane-bound G-protein receptor, Kiss1R, is located in the smooth muscle layer of uterine vessels, and that the peptide, Kiss, is produced by the rat placenta during late gestation. Kiss has been shown to produce vascular smooth muscle contraction in human aorta and coronary artery (Mead *et al.*, 2007). Our proposed model of how Kiss and Kiss1R interact within the uteroplacental unit during gestation in the rat is illustrated in Figure 7. Kiss, which is synthesized by the trophoblast cells of the placenta, binds to the Kiss1R in the arteries within the uterine vessels and mesometrial triangle to cause vasoconstriction.

Maternal ENM inhalation exposure during gestation alters uterine vascular Kiss reactivity. We hypothesize that potential blood flow decreases to the placental units is due to augmented vasoconstriction via Kiss-dependent mechanism. This would ultimately decrease pup weight and placental efficiency. In order to better understand the role of Kiss, microvascular reactivity within the uterus and placenta should also be evaluated during discrete developmental windows throughout gestation. Identifying such crucial windows when maternal nano-TiO_2 inhalation exposure augments effects of Kiss would allow for development of potential treatments for vascular-related gestational complications such as preeclampsia.

In conclusion, these studies represent the first evidence that pulmonary ENM exposure perturbs the normal gestational endocrine vascular axis, which is characterized by an augmented vascular Kiss reactivity. Additionally, fetal mass is decreased in combination with an enlarged placental size leading to placental inefficiency due to maternal ENM exposure during gestation. Size at birth is critical in determining health and life expectancy. Therefore, maternal ENM exposure during gestation has the potential to affect offspring health well into adulthood. Identifying perturbations in the reproductive, endocrine, and vascular axes that occur as a result of maternal ENM exposure during gestation and persist into adulthood are critical components in our understanding of the complex mechanisms of DOHaD.

DECLARATION OF CONFLICTING INTERESTS

The author(s) declared no potential conflicts of interest with respect to the research, authorship, and/or publication of this article.

ACKNOWLEDGMENTS

The authors thank the West Virginia University Imaging Facilities where imaging experiments and image analysis were performed and have been supported by the WVU Cancer Institute and NIH (P20RR016440 and P30RR032138/P30GM103488).

FUNDING

National Institutes of Health (R01-ES015022 to T.R.N.) and the National Science Foundation Cooperative Agreement (1003907 to T.R.N. and A.B.A.).

REFERENCES

Abukabda, A. B., Bowdridge, E. C., McBride, C. R., Batchelor, T. P., Goldsmith, W. T., Garner, K. L., Friend, S., and Nurkiewicz, T. R. (2019). Maternal titanium dioxide nanomaterial inhalation exposure compromises placental hemodynamics. *Toxicol. Appl. Pharmacol.* **367**, 51–61.

Abukabda, A. B., McBride, C. R., Batchelor, T. P., Goldsmith, W. T., Bowdridge, E. C., Garner, K. L., Friend, S., and Nurkiewicz, T. R. (2018). Group II innate lymphoid cells and microvascular dysfunction from pulmonary titanium dioxide nanoparticle exposure. *Part. Fibre Toxicol.* **15**, 43.

Abukabda, A. B., Stapleton, P. A., McBride, C. R., Yi, J., and Nurkiewicz, T. R. (2017). Heterogeneous vascular bed responses to pulmonary titanium dioxide nanoparticle exposure. *Front. Cardiovasc. Med.* **4**, 33.

Barker, D. J. (1990). The fetal and infant origins of adult disease. *BMJ* **301**, 1111.

Barker, D. J., and Martyn, C. N. (1992). The maternal and fetal origins of cardiovascular disease. *J. Epidemiol. Commun. Health* **46**, 8–11.

Bilban, M., Ghaffari, T. N., Hintermann, E., Bauer, S., Molzer, S., Zoratti, C., Malli, R., Sharabi, A., Hiden, U., Graier, W., *et al.* (2004). Kisspeptin-10, a KiSS-1/metastin-derived decapeptide, is a physiological invasion inhibitor of primary human trophoblasts. *J. Cell Sci.* **117**, 1319–1328.

Campagnolo, L., Massimiani, M., Vecchione, L., Piccirilli, D., Toschi, N., Magrini, A., Bonanno, E., Scimeca, M., Castagnozzi, L., Buonanno, G., *et al.* (2017). Silver nanoparticles inhaled during pregnancy reach and affect the placenta and the foetus. *Nanotoxicology* **11**, 687–698.

Castellano, J. M., Bentsen, A. H., Mikkelsen, J. D., and Tena-Sempere, M. (2010). Kisspeptins: Bridging energy homeostasis and reproduction. *Brain Res.* **1364**, 129–138.

Ćetković, A., Miljic, D., Ljubić, A., Patterson, M., Ghatei, M., Stamenković, J., Nikolic-Djurovic, M., Pekic, S., Doknic, M., Glišić, A., *et al.* (2012). Plasma kisspeptin levels in pregnancies with diabetes and hypertensive disease as a potential marker of placental dysfunction and adverse perinatal outcome. *Endocr. Res.* **37**, 78–88.

d'Anglemont de Tassigny, X., and Colledge, W. H. (2010). The role of kisspeptin signaling in reproduction. *Physiology* **25**, 207–217.

Department of Health and Human Services, Centers for Disease Control and Prevention, National Institute for Occupational Safety and Health. (2011) Occupational exposure to titanium dioxide. *Curr. Intell. Bull.* **63**, 1–140. www.cdc.gov/niosh/docs/2011-160/pdfs/2011-160.pdf. Accessed March 26, 2019.

de Roux, N., Genin, E., Carel, J. C., Matsuda, F., Chaussain, J. L., and Milgrom, E. (2003). Hypogonadotropic hypogonadism due to loss of function of the KiSS1-derived peptide receptor GPR54. *Proc. Natl. Acad. Sci. U.S.A.* **100**, 10972–10976.

Fowden, A. L., Sibley, C., Reik, W., and Constancia, M. (2006). Imprinted genes, placental development and fetal growth. *Hormone Res.* **65**(Suppl. 3), 50–58.

Gao, G., Ze, Y., Li, B., Zhao, X., Zhang, T., Sheng, L., Hu, R., Gui, S., Sang, X., Sun, Q., *et al.* (2012). Ovarian dysfunction and gene-expressed characteristics of female mice caused by long-term exposure to titanium dioxide nanoparticles. *J. Hazard. Mater.* **243**, 19–27.

Hafez, S. (2017). Comparative placental anatomy: Divergent structures serving a common purpose. *Prog. Mol. Biol. Transl. Sci.* **145**, 1–28.

Heath,J. R. (2015). Nanotechnologies for biomedical science and translational medicine. *Proc. Natl. Acad. Sci. U.S.A.* **112**, 14436–14443.

Hendren, C. O., Mesnard, X., Dröge, J., and Wiesner, M. R. (2011). Estimating production data for five engineered nanomaterials as a basis for exposure assessment. *Environ. Sci. Technol.* **45**, 2562–2569.

Hou, J., Wan, X., Wang, F., Xu, G., Liu, Z., and Zhang, T. (2009). Effects of titanium dioxide nanoparticles on development and maturation of rat preantral follicle in vitro. *Acad. J. Sec. Milit. Med. Univ.* **30**, 869–873.

Kotani, M., Detheux, M., Vandenbogaerde, A., Communi, D., Vanderwinden, J. M., Le Poul, E., Brézillon, S., Tyldesley, R., Suarez-Huerta, N., Vandeput, F., *et al.* (2001). The metastasis suppressor gene KiSS-1 encodes kisspeptins, the natural ligands of the orphan G protein-coupled receptor GPR54. *J. Biol. Chem.* **276**, 34631–34636.

Larson, J. K., Carvan, M. J., and Hutz, R. J. (2014). Engineered nanomaterials: An emerging class of novel endocrine disruptors. *Biol. Reprod.* **91**, 20,1–8.

Lehman, M. N., Coolen, L. M., Steiner, R. A., Neal-Perry, G., Wang, L., Moenter, S. M., Moore, A. M., Goodman, R. L., Yeo, S.-H., Padilla, S. L., *et al.* (2018). The 3rd World Conference on Kisspeptin, "Kisspeptin 2017: Brain and Beyond": Unresolved questions, challenges and future directions for the field. *J. Neuroendocrinol.* **30**, e12600.

Li, Y., Li, X. H., and Yuan, H. (2012). Angiotensin II type-2 receptor-specific effects on the cardiovascular system. *Cardiovasc. Diagn. Ther.* **2**, 56–62.

Mandala,M., and Osol,G. (2012). Physiological remodelling of the maternal uterine circulation during pregnancy. *Basic Clin. Pharmacol. Toxicol.* **110**, 12–18.

Mead, E. J., Maguire, J. J., Kuc, R. E., and Davenport, A. P. (2007). Kisspeptins are novel potent vasoconstrictors in humans, with a discrete localization of their receptor, G protein-coupled receptor 54, to atherosclerosis-prone vessels. *Endocrinology* **148**, 140–147.

Millar, R. P., and Babwah, A. V. (2015). KISS1R: Hallmarks of an effective regulator of the neuroendocrine axis. *Neuroendocrinology* **101**, 193–210.

Nurkiewicz, T. R., Porter, D.W., Hubbs, A.F., Cumpston, J.L., Chen, B.T., Frazer, D.G. and Castranova, V. (2008). Nanoparticle inhalation augments particle-dependent systemic microvascular dysfunction. *Particle and fibre toxicology*, **5**, 1.

Osol, G., and Mandala, M. (2009). Maternal uterine vascular remodeling during pregnancy. *Physiology* **24**, 58–71.

Qaiser, F., Wahab, F., Wiqar, M. A., Hashim, R., Leprince, J., Vaudry, H., Tena-Sempere, M., and Shahab, M. (2012). Study of the role of novel RF-amide neuropeptides in affecting growth hormone secretion in a representative non-human primate (*Macaca mulatta*). *Endocrine* **42**, 658.

Ramsden, C. S., Henry, T. B., and Handy, R. D. (2013). Sub-lethal effects of titanium dioxide nanoparticles on the physiology and reproduction of zebrafish. *Aquat. Toxicol.* **126**, 404–413.

Rennie, M. Y., Cahill, L. S., Adamson, S. L., and Sled, J. G. (2017). Arterio-venous fetoplacental vascular geometry and hemodynamics in the mouse placenta. *Placenta* **58**, 46–51.

Reynolds, L. P., and Redmer, D. A. (1992). Growth and microvascular development of the uterus during early pregnancy in ewes. *Biol. Reprod.* **47**, 698–708.

Stapleton, P. A., McBride, C. R., Yi, J., Abukabda, A. B., and Nurkiewicz, T. R. (2018). Estrous cycle-dependent modulation of in vivo microvascular dysfunction after nanomaterial inhalation. *Reprod. Toxicol.* **78**, 20–28.p

Stapleton, P. A., Minarchick, V. C., Yi, J., Engels, K., McBride, C. R., and Nurkiewicz, T. R. (2013). Maternal engineered nanomaterial exposure and fetal microvascular function: Does the Barker hypothesis apply? *Am. J. Obstet. Gynecol.* **209**, 227.e1–11.

Stapleton, P. A., and Nurkiewicz, T. R. (2014). Maternal nanomaterial exposure: A double threat to maternal uterine health and fetal development? *Nanomedicine* **9**, 929–931.

VanBavel, E. D., and Mulvany, M. J. (1994). Role of wall tension in the vasoconstrictor response of cannulated rat mesenteric small arteries. *J. Physiol.* **477**, 103–115.

Wilson, M. E., and Ford, S. P. (2001). Comparative aspects of placental efficiency. *Reprod. Suppl.* **58**, 223–232.

Yamashita, K., Yoshioka, Y., Higashisaka, K., Mimura, K., Morishita, Y., Nozaki, M., Yoshida, T., Ogura, T., Nabeshi, H., Nagano, K., *et al.* (2011). Silica and titanium dioxide nanoparticles cause pregnancy complications in mice. *Nat. Nanotechnol.* **6**, 321–328.

Yi, J. (2013). Whole-body nanoparticle aerosol inhalation exposures. *J. Vis. Exp.* e50263.